CHEMICAL ENGINEERING TRANSACTIONS
VOL. 100, 2023
A publication of AIDIC
The Italian Association of Chemical Engineering
Online at www.cetjournal.it
Guest Editors: Sauro Pierucci, Flavio Manenti

ISBN 979-12-81206-03-8; **ISSN** 2283-9216
DOI: 10.3303/CET23100021

Discrete Element Method Simulations of an Innovative Magnetic Stirred Device for the Top-down Production of Ferromagnetic Nanoparticles

Marco Trofa[a], Andrea Pietro Reverberi[b], Marco Vocciante[b,*]

[a]Scuola Superiore Meridionale, Largo San Marcellino 10, 80138, Napoli, Italy.
[b]DCCI, Dipartimento di Chimica e Chimica Industriale, Università degli Studi di Genova, Via Dodecaneso 31, 16146 Genova, Italy.
marco.vocciante@unige.it

Nanoparticles (NPs) are relevant in several industrial applications due to their peculiar properties with respect to their bulk precursor material. Hence, there is a growing need to develop novel technical solutions to synthetize such NPs by simple, eco-friendly, and cost-effective processes. In this regard, the authors have recently proposed a strategy for the safe and sustainable production of NPs involving a mechanical refining using magnetic agitation in wet-operating stirred media, which minimizes the NPs air dispersion and improves the control over the final product specifics. However, the magnetic agitation poses heavy limits of applicability in the case of synthesis of ferromagnetic NPs. In the present contribution, an alternative device configuration developed to overcome this limitation is investigated though a numerical approach. Discrete element method (DEM) simulations are performed to model the grinding and primary particles collisions and to clarify the effect of the parameters involved in both process setup and operation. The results are reported in terms of frequency and velocity of collision and compared to those of the standard device configuration to derive useful information about the functioning and capabilities of the novel system.

1. Introduction

Nowadays, nanoparticles (NPs) and nanostructured materials play a central role in the scientific landscape due to their special properties and versatility in a wide variety of unique applications, exploiting features such as enhanced chemical reactivity and catalytic capacity (Wang et al., 2015) resulting from their high surface-to-volume ratio. Examples include medical, industrial (Fabiano et al., 2015), and environmental (Alberti et al., 2021) applications, to name a few.

So far, the most common NPs synthesis strategies are based on bottom-up approaches, i.e., by progressive aggregation around seeds (e.g., ions or molecules). While it is easier to monitor the size of the final product (Reverberi et al., 2021), these methods often require the use of various chemicals, which can have toxic effects on humans and the environment.

In response to increasingly stringent constraints on environmental sustainability (Meramo et al., 2018), aiming for example to carbon neutrality, new approaches and procedures that generally refer to "green nanotechnology" (Reverberi et al., 2017) are constantly being developed. Among them, top-down synthesis methods, i.e., by disaggregation from macroscopic-sized elements or compounds subjected to physical treatment without any chemical reaction, are attracting increasing interest (Reverberi et al., 2021). Several disaggregation techniques have been proposed (Ogi et al., 2017), including the possible use of grinding media, such as beads. However, the lack of control over the size of the formed NPs (broad distribution) is still a drawback of these methods, which require the adoption of specific strategies, including the use of stabilizing agents to manage the tendency of the produced nanoparticles to re-aggregate (Ullah et al., 2014).

Recently, a top-down physical method has been developed based on mechanical refinement in wet stirred media, which, despite its simplicity, shows particularly promising results in terms of product quality, while remaining inherently safe, environmentally friendly, and economically viable (Reverberi et al., 2020). A crucial

Paper Received: 9 January 2023; Revised: 14 April 2023; Accepted: 17 May 2023
Please cite this article as: Trofa M., Reverberi A.P., Vocciante M., 2023, Discrete Element Method Simulations of an Innovative Magnetic Stirred Device for the Top-down Production of Ferromagnetic Nanoparticles, Chemical Engineering Transactions, 100, 121-126 DOI:10.3303/CET23100021

aspect of this process is the establishment of special operating conditions that enable a one-pot bead milling process, in which NPs are produced as a suspended phase in the process solvent directly from a bulky solid such as millimeter-sized metal spheres, minimizing NPs air dispersion and the need for stabilizers or separation steps. In addition to the mentioned advantages in terms of safety and practicality, noteworthy is the ability of such a configuration to overcome a well-known rule of thumb established for this type of processes. Indeed, it is possible to produce particles with a size reduction factor of $1/10^5$ with respect to the precursor beads, instead of the expected literature limit of 1/1000 (Reverberi et al. 2020).
However, the magnetic agitation underlying the functioning of the system poses strong limitations to the synthesis of ferromagnetic NPs. To overcome such problem, while preserving the pros of the discussed approach, an alternative device configuration has been developed. In this new setup the stirring is obtained through an impeller connected to a magnetic bar which is kept outside of the fluid containing the precursor beads. In this way, no magnetization is induced in case of ferromagnetic NPs, thus limiting aggregation, and favoring the achievement of a homogeneous and more stable dispersion. In addition, the impeller shaft is completely confined inside the vessel, thus overcoming the shaft sealing problem and allowing the operation under pressure and/or with volatile solvents, with clear safety and environmental advantages. This particular expedient is also appropriate for one-pot purification processes, where NPs are employed as soon as they are synthesized (like in the abatement of chlorinated hydrocarbons with zerovalent iron NPs), with considerable savings in the costs related to equipment and safety.
In this contribution, the new configuration still under development (Reverberi et al., 2022) is investigated by means of numerical simulations. The primary purpose is to highlight the effect of the changes in the experimental apparatus on the system dynamics and ultimately on the efficiency of the abrasion process underlying the generation of NPs. For ease of comparison, the same synthesis of silver NPs previously numerically investigated in the standard apparatus (Trofa and Vocciante, 2020) is considered. As before, the dynamics of the system is expected to be mainly governed by particle-particle collisions. Hence, the process is modeled through the Discrete Element Method (DEM), which allows to obtain, albeit as first approximation, the motion of the grinding and precursor beads, and provide useful information on the collision frequency and impact velocities.

2. Materials and methods

2.1 Experimental set-up

The main characteristics of the novel customary-made wet milling device setup, schematically reported in Figure 1a, are the following:

- cylindrical container (height 120 mm, internal diameter 31 mm, glass);
- cylindrical magnetic bar (hemispherical ends, length 30 mm, diameter 5 mm, PTFE coating);
- L-bent rotating shaft (hemispherical end, diameter 5 mm, L-arm length 11 mm, glass);
- four silver beads (diameter 3 mm, Ag 99.9% (American Elements));
- forty beads of yttria-stabilized zirconia (diameter 3 mm, ZrO_2 95%, Y_2O_3 5% (MSE Supplies)).

The metal precursor undergoing disaggregation (silver beads) and the grinding media (zirconia beads) are kept in motion by the L-bent rotating glass shaft, coated at the bottom end with PTFE (to minimize shear stresses between the relative moving parts), which is driven at its top by the aforementioned magnetic bar. The electrically powered magnetic trailing device is positioned above the top of the miller. The rotation induces collisions among the beads and the consequent abrasion of the metal precursor with the release of silver NPs. The detailed description of the experimental apparatus mentioned above can be found in Reverberi et al. (2022). The most relevant structural variation with respect to the one previously investigated (Trofa and Vocciante, 2020) is the position of the magnetic bar, in this case operating outside the liquid containing the beads. This configuration is elsewhere referred to as outer-bar wet miller (OWM), while the original configuration as inner-bar wet miller (IWM) (Reverberi et al. 2022).
Regardless of the configuration considered, the wet grinding process does not start or is subject to a random stop when the number of beads contained in the vessel exceeds a certain threshold. This occurs when the resistance torque exerted by the beads on the immersed bar (IWM) or moving shaft (OWM) is greater than the driving torque applied by the magnetic traction. Since the magnetic bar immersed obliquely in the IWM has a lower torque than an identical magnetic bar rotating horizontally in the OWM, the new configuration has a lower tendency to jam and can be more easily employed in autogenous grinding, that is, when only metal precursor spheres are used in the absence of ZrO_2 (generally having a lower specific gravity and thus minor inertia).
In contrast, in the OWM, careful control of the clearance between the shaft and the inner surface of the vessel, both in the horizontal and vertical directions, is required to prevent shaft jamming and abrupt seizure. This constraint implies greater design complexity, but it is more than offset by the advantages offered, leading to significantly higher hourly output of metallic NPs in the case of OWM.

Most importantly, as mentioned above, a unique advantage offered by the OWM scheme is that it can be used for the disaggregation of ferromagnetic materials to produce the corresponding NPs. Such a process could not be performed with IWM, as the bulky metal and the released NPs would be attracted by the magnetic field created by both the stirring bar and the external drag device, resulting in a drastic loss of grinding efficiency and magnetism-induced aggregation of the NPs.

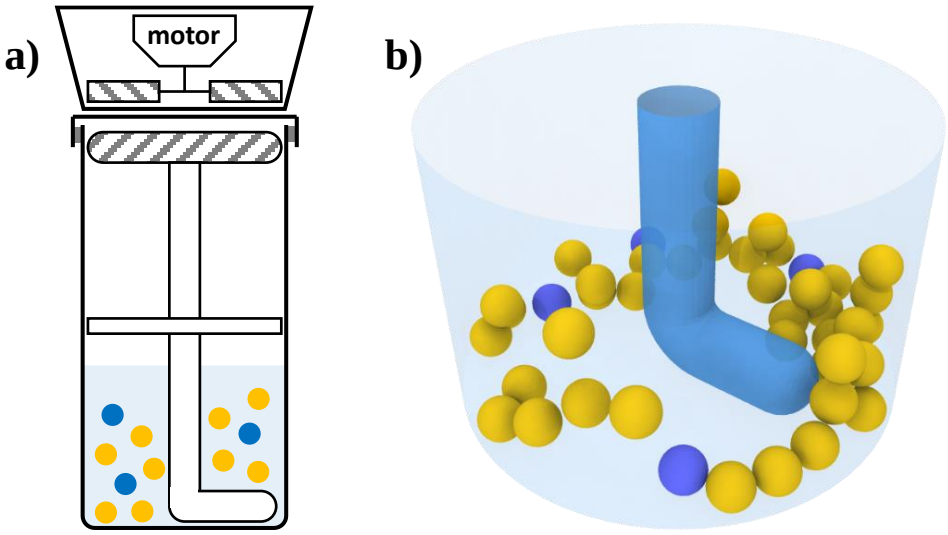

Figure 1: (a) Schematic representation of the outer-bar wet miller OWM. (b) Snapshoot of the simulation domain showing the L-bent rotating glass shaft stirring the beads (yellow for ZrO_2 and blue for Ag).

2.2 Numerical set-up

A sketch of the computational domain used to perform the numerical study is reported in Figure 1b. In the system, the yellow and blue beads indicate ZrO_2 and Ag particles, respectively. The motion is imposed through the counterclockwise rotation of the L-bent glass shaft at three different angular velocities 300, 600, and 900 rpm. The dynamics of the particles is tracked by explicitly solving their trajectories using the Discrete Element Method (Marshall and Li, 2014), i.e., by solving the force and torque balance on each particle:

$$m_\mathrm{p}\frac{d\boldsymbol{u}_\mathrm{p}}{dt} = \sum_j \boldsymbol{F}_\mathrm{c} + m_\mathrm{p}\boldsymbol{g}, \quad I_\mathrm{p}\frac{d\boldsymbol{\omega}_\mathrm{p}}{dt} = \sum_j \boldsymbol{T}_\mathrm{c} \tag{1}$$

In (1) $\boldsymbol{u}_\mathrm{p}$ and $\boldsymbol{\omega}_\mathrm{p}$ are the translational and angular velocity, while m_p, and I_p represent particle mass and moment of inertia, respectively. Finally, $\boldsymbol{F}_\mathrm{c}$ and $\boldsymbol{T}_\mathrm{c}$ are the contact force and torque acting on a given particle due to other particles or walls, calculated according to the Hertz-Mindlin model (Vocciante et al., 2019), while $\boldsymbol{g}$ is the gravity force. By integrating the kinematic equations (2), it is then possible to obtain the updated position $\boldsymbol{x}_\mathrm{p}$ and angular position $\boldsymbol{\theta}_\mathrm{p}$ of the particle.

$$\frac{d\boldsymbol{x}_\mathrm{p}}{dt} = \boldsymbol{u}_\mathrm{p}, \quad \frac{d\boldsymbol{\theta}_\mathrm{p}}{dt} = \boldsymbol{\omega}_\mathrm{p} \tag{2}$$

The properties of the considered materials are listed in Table 1 and have been taken from the literature (see Fragnière et al. (2018) for zirconia and glass, Smith and Fickett (1995) for silver, and Gondret et al. (2002) for PTFE).

Table 1: Model parameters and material properties (adapted from Trofa and Vocciante, 2020)

	Zirconia, ZrO_2	Silver, Ag	Glass	PTFE
Density [kg/m^3]	6067	10490	2510	2200
Young's Modulus [GPa]	210.0	82.0	70.0	0.50
Poisson ratio	0.31	0.36	0.24	0.46
Coefficient of restitution	0.92	0.80	0.99	0.80
Coefficient of friction	0.15	0.55	0.27	0.08

The system is initialized by randomly placing the beads into the container and then letting them free fall for 0.5 s. Then the sampling of the contacts is performed for 5 s. To ensure statistical invariance from the insertion procedure, the results presented are obtained by averaging over six simulations with different initial random particle distributions.
The collisions are identified by the changes in contacts among particles and walls at every time step through a customized procedure that, identifying the new contacts and detachments, allows for a proper analysing of the number and relative velocity of collisions (Vocciante et al., 2019).
The time step for the numerical integration is set to 10^{-7} s. This value is sufficiently smaller than the actual collision time (whose scale is given by Rayleigh and Hertz times), thus ensuring a proper resolution of the impact dynamics and the stability of numerical simulations (Marshall and Li, 2014). The open-source software LIGGGHTS® 3.8.0 has been used to implement and execute the code (more details can be found in Kloss et al. (2012)).

3. Results

The total translational ($ke = 0.5\sum m_\mathrm{p} u_\mathrm{p}^2$) and rotational ($ke_\mathrm{rot} = 0.5\sum I_\mathrm{p}\omega_\mathrm{p}^2$) kinetic energy of the system are shown in Figures 2a and 2b, respectively. As mentioned, the data for each of the three stirring velocities reported are obtained by averaging over six simulations with different initial random particle distributions. Similarly to the previous case (Trofa and Vocciante, 2020) the system presents an initial transient with an energy peak due to the initialization procedure and then achieves a pseudo steady-state regime, i.e., with an almost constant mean value proportional to the rotational velocity. The translational energy starts from a finite value since the particles are initialized with a finite falling speed, whereas the rotational energy is zero. As compared to the corresponding IWM, with the same beads and rotational velocity, both energies are increased by a factor around two, due to the higher tip-speed connected to the longer stirring arm. In the stable regime the collisions per second are around 10300, 3400, 2500 for the cases 300, 600, and 900 rpm, respectively.

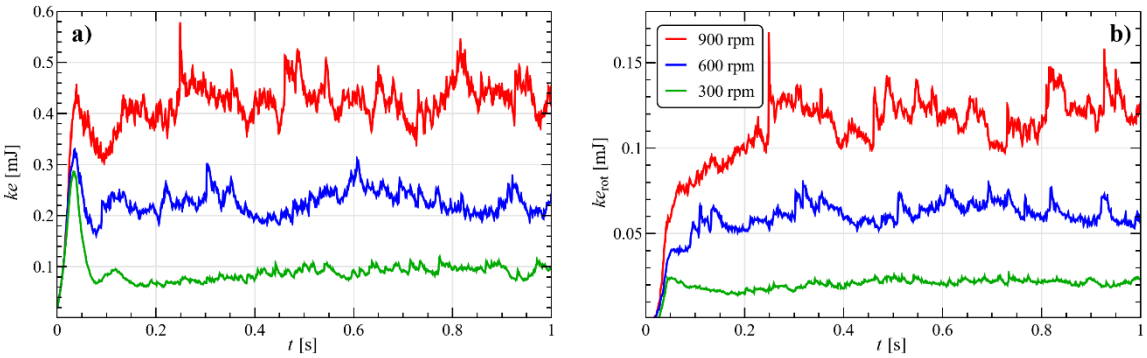

Figure 2: Total translational (a) and rotational (b) kinetic energy for different stirring velocities. Data are obtained by averaging over six simulations with different initial random particle distributions.

In Figure 3 (left) the collisions duration and (right) the normal component of the relative velocity at the beginning of a contact $u_\mathrm{r,n} = \left(\boldsymbol{u}_\mathrm{p,i} - \boldsymbol{u}_\mathrm{p,j}\right)\cdot\boldsymbol{n}$, with $\boldsymbol{n}$ the normal vector to the contact plane, are shown. Data are reported in terms of probability, i.e., the fraction of data corresponding to each bin, for all the particles in the system (a-b), and for the collisions involving at least a silver particle (c-d). The dashed lines denote the medians of the distributions, which turn to be all unimodal.
Since even the shortest collision (900 rpm in Figure 3a) lasts approximately 80 time steps (i.e., 8 μs), a fine resolution of the contacts is ensured. At decreasing rotational velocity (600 and 300 rpm in Figure 3a), the distribution median shifts to higher values and the variance increases. This growth in the collisions duration is connected to a reduction of the particles translational velocity and in turn of their relative and collisional velocity (Figure 3b). The impacts involving at least a silver particle (Figure 3c-d) and the ones with the container walls (not shown) present the same general trend. However, due to the lower Young modulus and restitution coefficient of silver and glass as compared to zirconia, these collisions result ‘softer’ and more dissipative, with a longer duration (Figure 3c), lower rebound velocity, and then lower impact speed (Figure 3d).

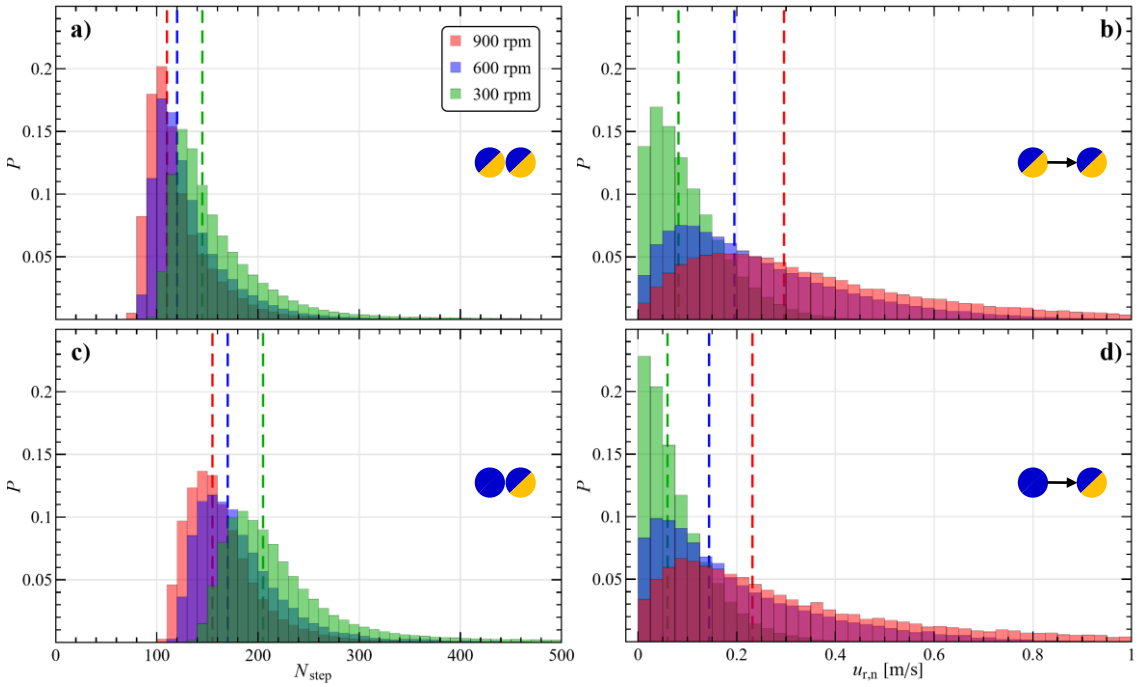

Figure 3: Probability distribution of the contact time and normal relative impact velocity among all the particles (a-b), and for the collisions involving at least a silver particle (c-d), for different stirring velocities.

Considering the collisions involving at least a silver particle, the tangential component of the relative impact velocity $u_{r,t} = \left\|(\boldsymbol{I} - \boldsymbol{nn}) \cdot (\boldsymbol{u}_{p,i} - \boldsymbol{u}_{p,j}) - r_p(\boldsymbol{\omega}_{p,i} + \boldsymbol{\omega}_{p,j}) \times \boldsymbol{n}\right\|$, with $\boldsymbol{I}$ the identity tensor and r_p the particle radius, is reported in Figure 4 for particle-particle (a) and particle-wall (b) collisions. Like $u_{r,n}$ (Figure 3d) also the distribution for $u_{r,t}$ (Figure 4a) is unimodal and spans a similar range, though the medians are nearly doubled and closer to the bar tip speed, which for instance is 0.7 m/s at 600 rpm. This means that the collisions are mainly tangential, with a median impact angle around 30 degrees.
Compared to the collisions among beads, those with the container walls have an almost doubled frequency (19600, 5700, 3900 for the cases 300, 600, and 900 rpm) but significantly lower velocities (Figure 4b). Indeed, the novel system is less packed and constrained by the side walls, hence the slower collisions with the vessel bottom are much more numerous than the faster ones with the side walls, which involve faster particles (closer to the tip speed) and are responsible for their change in direction.

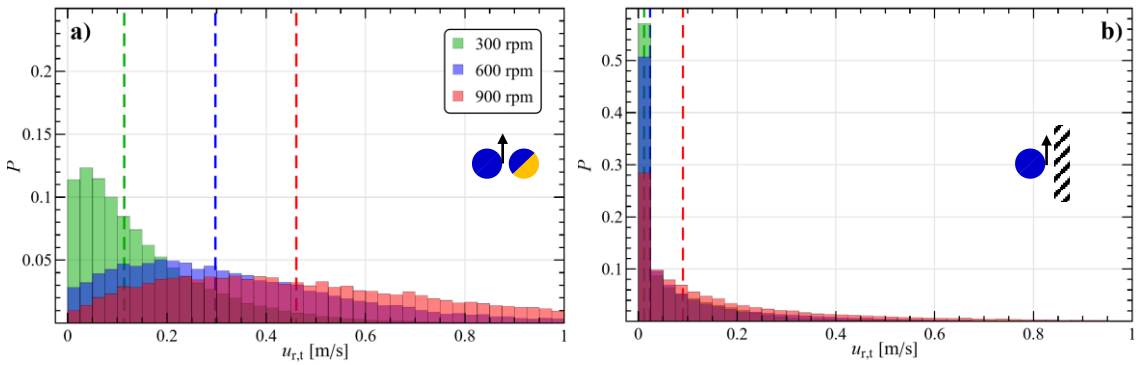

Figure 4: Probability distribution of the tangential relative impact velocity involving at least a silver particle (a), and with the container wall (b), for different stirring velocities.

A comparison with the previous IWM configuration (Trofa and Vocciante, 2020) shows that the new OWM system is not only more energetic by a factor of around two (Figure 2), which is connected to an increase in the particle translational and rotational velocities, but also the impact speed among them increases (Figure 3b).

Specifically, in the new configuration the normal component of the collision velocity grows by almost an order of magnitude, while the tangential component grows less than a factor two. Hence the collisions are more ‘normal’, as confirmed by the impact angle (not shown) whose median increases from about 15 (Trofa et al., 2020) to 30 degrees.

4. Conclusions

In this contribution, a novel device configuration for the production of metal NPs is investigated through DEM numerical simulations. The system is characterized by the possibility to obtain ferromagnetic NPs despite the magnetic induced stirring. Three different rotational velocities are considered, with an in-depth analysis of the particles impacts.

Regardless of the stirring velocity, in the range investigated the system presents a stable dynamics, with a nearly constant kinetic energy and collision frequency. Although to a lesser extent than in the inner-bar wet miller (IWM) configuration, due to an increased normal impact velocity, the beads collisions are still characterized by a prevalent tangential component, attesting that the shear among particles is the main responsible for abrasion in the actual process.

The investigation of different device configurations, system materials, and operative conditions, performed both through experiments and numerical simulations represents a useful contribution towards the implementation a more efficient, economical, inherent safe, and eco-friendly multi-scale approach for NPs production.

References

Alberti S., Basciu I., Vocciante M., Ferretti M., 2021, Experimental and physico-chemical comparison of ZnO nanoparticles’ activity for photocatalytic applications in wastewater treatment, Catalysts, *11*(6), 678.

Fabiano B., Pistritto F., Reverberi A., Palazzi E., 2015, Ethylene-air mixtures under flowing conditions: a model-based approach to explosion conditions, Clean Technologies and Environmental Policy 17, 1261–1270.

Fragnière G., Beinert S., Overbeck A., Kampen I., Schilde C., Kwade A., 2018, Predicting effects of operating condition variations on breakage rates in stirred media mills, Chemical Engineering Research and Design, 138, 433–443.

Gondret P., Lance M., Petit L., 2002, Bouncing motion of spherical particles in fluids, Physics of fluids, 14(2), 643–652.

Kloss C., Goniva C., Hager A., Amberger S., Pirker S., 2012, Models, algorithms and validation for opensource DEM and CFD–DEM, Progress in Computational Fluid Dynamics, an International Journal 12(2-3), 140–152.

Marshall J.S., Li S., 2014, Adhesive particle flow, Cambridge University Press, New York, USA.

Meramo S.I., Bonfante H., De Avila-Montiel G., Herrera-Barros A., Gonzalez-Delgado A., 2018, Environmental assessment of a large-scale production of TiO_2 nanoparticles via green chemistry, Chemical Engineering Transactions, 70, 1063–1068.

Ogi T., Zulhijah R., Iwaki T., Okuyama K., 2017, Recent progress in nanoparticle dispersion using bead mill, KONA Powder and Particle Journal, 34, 3–23.

Reverberi A.P., Vocciante M., Lunghi E., Pietrelli L., Fabiano B., 2017, New Trends in the Synthesis of Nanoparticles by Green Methods, Chemical Engineering Transactions, 61, 667–672.

Reverberi A.P., Vocciante M., Salerno M., Ferretti M., Fabiano B., 2020, Green synthesis of silver nanoparticles by low-energy wet bead milling of metal spheres, Materials, 13(1), 63.

Reverberi A. P., Salerno M., Vocciante M., Trofa M., Fabiano, B., 2021, Gallium nanoparticles by surface wet disaggregation and abrasion, Chemical Engineering Transactions, 86, 787–792.

Reverberi A.P., Vocciante M., Salerno M., Soda O., Fabiano B., 2022, A sustainable, top-down mechanosynthesis of carbohydrate-functionalized silver nanoparticles, Reaction Chemistry & Engineering, *7*(4), 888–897.

Smith D.R., Fickett F.R., 1995, Low-temperature properties of silver, Journal of Research of the National Institute of Standards and Technology, 100(2), 119–171.

Trofa, M., D’Avino, G., Fabiano, B., & Vocciante, M. (2020). Nanoparticles synthesis in wet-operating stirred media: Investigation on the grinding efficiency. *Materials*, *13*(19), 4281.

Trofa M., Vocciante M., 2020, Discrete element simulations of nanoparticles synthesis in wet-operating stirred media: Effect of the particle material, Chemical Engineering Transactions, *82*, 385–390.

Ullah M., Ali M.E., Hamid S.B.A., 2014, Surfactant-assisted ball milling: A novel route to novel materials with controlled nanostructure - A review, Review on Advanced Materials Science, 37, 1–14.

Vocciante M., Trofa M., D’Avino G., Reverberi A.P., 2019, Nanoparticles Synthesis in Wet-operating Stirred Media: Preliminary Investigation with DEM Simulations, Chemical Engineering Transactions, 74, 31–36.

Wang J., Gu H., 2015, Novel metal nanomaterials and their catalytic applications, Molecules 20, 17070–17092.